An Integrin Phosphorylation Switch
THE EFFECT OF β3 INTEGRIN TAIL PHOSPHORYLATION ON DOK1 AND TALIN BINDING*[S]◆

Camilla L. Oxley, Nicholas J. Anthis, Edward D. Lowe, Ioannis Vakonakis, Iain D. Campbell, and Kate L. Wegener[1]
From the Department of Biochemistry, University of Oxford, South Parks Road, Oxford OX1 3QU, United Kingdom

Integrins play a fundamental role in cell migration and adhesion; knowledge of how they are regulated and controlled is vital for understanding these processes. Recent work showed that Dok1 negatively regulates integrin activation, presumably by competition with talin. To understand how this occurs, we used NMR spectroscopy and x-ray crystallography to investigate the molecular details of interactions with integrins. The binding affinities of β3 integrin tails for the Dok1 and talin phosphotyrosine binding domains were quantified using ^{15}N-^{1}H heteronuclear single quantum correlation titrations, revealing that the unphosphorylated integrin tail binds more strongly to talin than Dok1. Chemical shift mapping showed that unlike talin, Dok1 exclusively interacts with the canonical NPXY motif of the β3 integrin tail. Upon phosphorylation of Tyr^{747} in the β3 integrin tail, however, Dok1 then binds much more strongly than talin. Thus, we show that phosphorylation of Tyr^{747} provides a switch for integrin ligand binding. This switch may represent an *in vivo* mechanism for control of integrin receptor activation. These results have implications for the control of integrin signaling by proteins containing phosphotyrosine binding domains.

Integrins are cell surface receptors that play key roles in cell migration and adhesion by providing a physical connection between the extracellular matrix and the cytoskeleton and transmitting signals through this connection. Thus, they have important functions in such biological processes as the immune response, leukocyte traffic, blood vessel development, hemostasis, and cancer (1). Integrins are heterodimers of an α and β subunit, each of which contains a large multidomain extracellular portion (>700 residues) and a short, largely unstructured cytoplasmic domain (13–70 residue), connected by a single transmembrane helix (2). Transmembrane signal transduction through the integrins can be conducted in either direction, in what is referred to as either outside-in or inside-out signaling.

Ligand binding to the cytoplasmic tails is an important step in bidirectional signaling and can control the activation states of integrins (3).

The integrin β subunit cytoplasmic tails are critical for integrin activation (4). They contain two NPXY or NPXY-like motifs, which have a propensity to form β turns (5) that bind to phosphotyrosine binding (PTB)[2] domains in a conserved peptide binding pocket (6). The talin PTB domain has, for example, been shown to bind to the NPLY motif in the β3 integrin subunit in this way. In addition, talin also uniquely recognizes a relatively independent binding site at the integrin membrane-proximal region, an interaction that is key to integrin activation (7).

The cytoplasmic protein Dok1 is involved in a variety of signaling pathways. It is a substrate of several other tyrosine kinases, suggesting that it has an important role in cell signaling (8) and cell migration (9). In chronic myelogenous leukemia, Dok1 is constitutively tyrosine-phosphorylated (10). It has been identified as a key down-regulator of cytokine responses and is essential for suppression of leukemia (11). To date, seven members of the Dok family have been identified (13) (14), each of which is comprised of an N-terminal pleckstrin homology domain followed by a PTB domain and a tyrosine and proline rich sequence near the C terminus.

Recently the Dok1 PTB domain has been shown to bind to β3 integrin tails (15), but in contrast to the talin PTB domain, Dok1 negatively regulates integrin activation (7). To investigate how this occurs, we set out to characterize the molecular basis of the interaction between the Dok1 PTB domain and the β3 integrin tail using NMR and x-ray crystallography. We show here that Dok1 binds specifically to the integrin NPLY motif and that this binding is positively regulated by tyrosine phosphorylation. In contrast, tyrosine phosphorylation has an inhibitory effect on talin binding. Thus, we show that, through opposing affinity effects, phosphorylation of β integrin Tyr^{747} will greatly increase the fraction of the Dok1-integrin complex while decreasing the fraction of talin-integrin complex; phosphorylation therefore could act as a "switch" that modulates integrin activation. These results have implications for other PTB domain-containing proteins and their possible interactions with β-integrin tails.

The atomic coordinates and structure factors (code 2v76) have been deposited in the Protein Data Bank, Research Collaboratory for Structural Bioinformatics, Rutgers University, New Brunswick, NJ (http://www.rcsb.org/).
[S] The on-line version of this article (available at http://www.jbc.org) contains a protein structure file.
[1] To whom correspondence should be addressed. Tel.: 44-1865-275772; Fax: 44-1865-275253; E-mail: kate.wegener@bioch.ox.ac.uk.

[2] The abbreviations used are: PTB, phosphotyrosine binding; HSQC, heteronuclear single quantum correlation; HPLC, high pressure liquid chromatography; pY, phosphotyrosine; MES, 4-morpholineethanesulfonic acid; IRS, insulin receptor substrate.

EXPERIMENTAL PROCEDURES

Preparation and Purification of Peptides and Proteins—Peptides derived from the $\beta 3$ integrin tail were synthesized commercially by EZBiolabs (Westfield, IN), GL Biochem (Shanghai, China), and GenScript (GenScript, Piscataway, NJ); they were assessed as >90% purity by high performance liquid chromatography, and their identities were confirmed by mass spectrometry.

U-^{15}N-labeled talin PTB domain and U-^{15}N-labeled and U-^{15}N,^{13}C Dok1 PTB domain were expressed and purified as described previously (7, 16). Unlabeled proteins were produced in a similar manner, but using Luria-Bertani broth rather than minimal medium.

The DNA sequence of the full-length $\beta 3$ integrin tail (Lys^{716}–Thr^{762}) was amplified and subcloned into a pET16b vector modified to contain a 3C protease cleavage site using the In-Fusion cloning system (Clontech). The U-^{15}N-labeled $\beta 3$ integrin tail was produced by *Escherichia coli* grown in M9 minimal medium with [^{15}N]ammonium chloride as the sole nitrogen source. Upon induction with 1 mM isopropyl-1-thio-β-D-galactopyranoside, the $\beta 3$ integrin tail was expressed insolubly, as inclusion bodies. The bacteria were lysed, and the integrin tail was purified under denaturing conditions (50 mM sodium phosphate, 300 mM NaCl, 8 M urea, pH 7.0) by Talon immobilized metal affinity chromatography (Clontech), eluting the polyhistidine-tagged integrin tail in 200 mM imidazole. Further purification was performed by C4 reverse phase HPLC. The polyhistidine tag was removed by cleavage with 3C protease, and the integrin tail was further purified by HPLC, leaving a construct with the sequence of the $\beta 3$ integrin tail, preceded by two amino acids from the vector (Gly-Pro).

NMR Spectroscopy—All NMR experiments were performed on spectrometers equipped with Oxford Instruments superconducting magnets (500, 600, and 750 MHz ^{1}H operating frequencies) and GE/Omega computers. Unless otherwise indicated, all samples were prepared in 50 mM phosphate buffer (pH 6.1), containing 100 mM NaCl and 5% D$_2$O. Complete protease inhibitors (Roche Applied Science) and sodium azide (final concentration 0.05%) were also present. The backbone signals of the Dok1 PTB domain were assigned using a sample of 1.5 mM [U-^{15}N/^{13}C]Dok1 PTB domain, employing standard techniques including three-dimensional CBCA(CO)NH and CBCANH experiments. The ^{1}H and ^{15}N resonances of U-^{15}N-labeled $\beta 3$ integrin tail were assigned using a 1 mM sample in 20 mM sodium acetate, pH 4.0, and employing three-dimensional nuclear Overhauser effect spectroscopy-HSQC and three-dimensional total correlation spectroscopy-HSQC spectra. Resonance assignments were then transferred to pH 6.1 through pH titrations. Spectra were referenced in the direct dimension either to the water signal (4.766 ppm ^{1}H ref at 25 °C) or to 2,2-dimethyl-2-silapentane-5-sulfonate sodium salt at 0 ppm, with indirect referencing in the ^{15}N dimension using a ^{15}N-^{1}H frequency ratio of 0.101329118 (17). Data were processed using NMRPipe (18) and spectra were visualized using the program SPARKY.

^{1}H-^{15}N HSQC titrations of U-^{15}N-labeled proteins (0.1 mM) with integrin peptides were performed as described previously

(16). Ligand concentrations (corrected for volume losses) were as follows: for Dok1 PTB domain and $\beta 3$ integrin peptide ^{736}RAKWDTANNPLYKE^{749}, 1.1, 2.3, 3.5, 5.4, 7.2, 9.8, 13.7, 18.9 mM; for Dok1 and pTyr^{747}-$\beta 3$ integrin ^{736}RAKWDTAN-NPL(pY)KE^{749}, 0.05, 0.1, 0.6, 1.1, 1.7 mM; for talin and ^{736}RAKWDTANNPLYKE^{749}, 1.0, 2.1, 3.2, 4.8, 6.5, 8.9, 12.5, 17.3 mM; for talin and ^{736}RAKWDTANNPL(pY)KE^{749}, 1.0, 2.1, 3.1, 4.8, 6.5, 8.8, 12.3, 17.1 mM. ^{1}H-^{15}N HSQC titrations of U-^{15}N-labeled full-length $\beta 3$ integrin tail were performed with 0.05 mM integrin tail and 0, 0.025, 0.05, 0.1, 0.2, 0.3, 0.4, 0.5, 0.6, 0.7, 0.8, or 1 mM Dok1 PTB or 0, 0.025, 0.05, 0.75, 0.1, 0.15, 0.25, 0.35, 0.5, 0.7, or 1 mM talin F3.

Weighted combined ^{1}H and ^{15}N amide shifts (Δ(H,N)) were calculated using the equation,

$$\Delta(\mathrm{H,N}) = \sqrt{\Delta_{\mathrm{H}}W_{\mathrm{H}}^2 + \Delta_{\mathrm{N}}W_{\mathrm{N}}^2} \qquad \text{(Eq. 1)}$$

where W_{H} and W_{N} are weighting factors for the ^{1}H and ^{15}N amide shifts, respectively ($W_{\mathrm{H}} = 1$, $W_{\mathrm{N}} = 0.154$) (19), and $\Delta = \delta_{\mathrm{bound}} - \delta_{\mathrm{free}}$. Dissociation constants (K_d) were determined by fitting changes in backbone chemical shift with concentration, to the following equation,

$$\Delta(\mathrm{H,N}) = \Delta(\mathrm{H,N})_0 \frac{[\mathrm{P}] + [\mathrm{L}] + K_d - \sqrt{([\mathrm{P}] + [\mathrm{L}] + K_d)^2 - 4[\mathrm{P}][\mathrm{L}]}}{2[\mathrm{P}]}$$

(Eq. 2)

where K_d is the dissociation constant, Δ(H,N) is the weighted shift change, Δ(H,N)$_0$ is the shift change at saturation, whereas [P] and [L] are the protein and ligand concentrations, respectively. Data from the highest signal-to-noise ratio peaks with the greatest shift changes were fit simultaneously to this equation with the program Origin (v7.0383, OriginLab Corp.), extracting a single K_d and multiple Δ(H,N)$_0$ values. Only peaks that were well resolved throughout the titration were used. Twenty-one peaks were used for Dok1 with the $\beta 3$ integrin peptide, 19 for Dok1 with pTyr^{747}-$\beta 3$ integrin, 22 for talin with $\beta 3$ integrin, and 19 for talin with pTyr^{747}-$\beta 3$ integrin. For the full-length $\beta 3$ integrin peptide with talin, 22 peaks were used, and seven peaks were used for the full-length $\beta 3$ integrin with Dok1.

Crystallization—Human Dok1 PTB domain was dialyzed into 10 mM MES, pH 6.5, 30 mM NaCl and concentrated to ~15 mg/ml. Crystals grew in 2 M NH$_4$SO$_4$, 2% polyethylene glycol 400 and 0.1 M Na-HEPES, pH 7.5, within 1 week at 20 °C.

Data Collection and Structure Determination—Data were collected at the European Synchrotron Radiation Facility (ESRF) on beamline ID14-EH2, and the crystal was flash-frozen in liquid nitrogen after soaking in a reservoir solution supplemented with 20% glycerol as a cryo-protectant. Data were indexed and integrated using MOSFLM and then scaled and merged using SCALA from the CCP4 program suite (20). The structure was phased by molecular replacement with the mouse Dok1 PTB domain (Protein Data Bank entry 1p5t) (21) as a search model and using the program Phaser (22). The crystal belonged to the space group C2, containing four molecules in the asymmetric unit and a solvent content of 48.6%. The electron density for the four molecules was averaged using the CCP4 program DM. After averaging, the model was rebuilt

using the program ARP/wARP. Further model building and refinement were carried out with the programs Coot (23) and Refmac.

Structural Modeling of the β3 Integrin Tail-Dok1 PTB Domain Complex—The crystal structure of the mouse Dok1 PTB domain in complex with the phosphorylated RET peptide (protein Data Bank number 1uef (21)) was aligned with the human Dok1 PTB domain structure. The atomic coordinates of the residues of the RET peptide were copied into the coordinate file of the human Dok1 PTB domain structure, and the side chains of the RET peptide were mutated to those of the β3 integrin tail using the program COOT from the CCP4 suit. This preliminary model was energy-minimized employing a simulated annealing protocol (initial temperature 5000 K) using PHENIX Refine (Python-based hierarchical environment for integrated Xtallography) (24).

Sequence Alignment—The alignment was generated using the protein structure comparison service SSM at European Bioinformatics Institute (25). A homology model of the MIG-2 PTB domain was generated using the talin PTB domain (Protein Data Bank entry 1y19) as a template and employing the program SWISS-MODEL (26). Graphical representation was achieved with the program ESPript (27).

Accession Numbers—Chemical shift assignments for the backbone resonances of the Dok1 PTB domain and full-length β3 integrin tail have been deposited in the BioMagResBank with the accession numbers 15551 and 15552, respectively. The coordinates of the human Dok1 PTB domain crystal structure were deposited in the Protein Data Bank with the ID code 2v76. The coordinates of the modeled integrin peptide-dok1 complex are included as supplemental data.

RESULTS

Dok1 and Talin PTB Domain Binding to Full-length β3 Integrin Tail—To understand the molecular mechanism by which Dok1 PTB negatively regulates integrin activation (7), we set out to determine the binding mode of the human Dok1 PTB domain to the β3 integrin tail using NMR. This was done by assigning the backbone resonances of the ^{15}N isotopically labeled full-length β3 integrin peptide in solution and then observing the amide chemical shift changes in ^{1}H-^{15}N HSQC NMR spectra upon the addition of unlabeled Dok1 PTB domain. Fig. 1A shows that the residues surrounding the NPLY region of β3 integrin are perturbed, whereas the membrane-proximal residues are unaffected. Following the chemical shift changes, as a function of ligand concentration, shows that the K_d of this interaction is at least several millimolars (Fig. 1B). A similar titration was performed for the β3 integrin tail with the talin PTB domain, and a K_d value of 223 ± 5 μM was calculated (Fig. 1B), revealing that talin has a higher affinity for unmodified β3 integrin tails than Dok1 by at least an order of magnitude.

Dok1 PTB Binding to β3 Integrin Tail and to Tyr(P)-747 β3 Integrin Tail—To determine the effect of β3 integrin tails on Dok1, similar NMR titrations were performed, this time using ^{15}N-labeled Dok1 and synthetic unlabeled integrin tail fragments. The chemical shifts of the Dok1 PTB domain backbone atoms were first assigned in the unbound state, before titrating in β3 integrin tail-derived peptides. All NMR spectra were con-
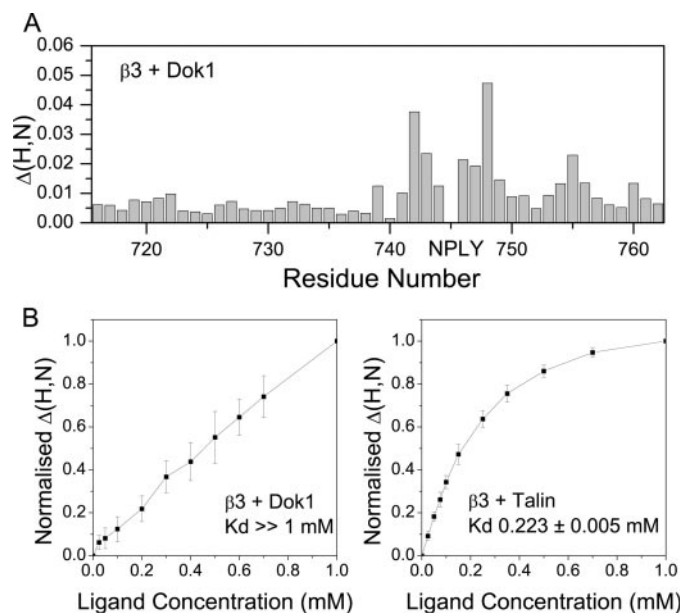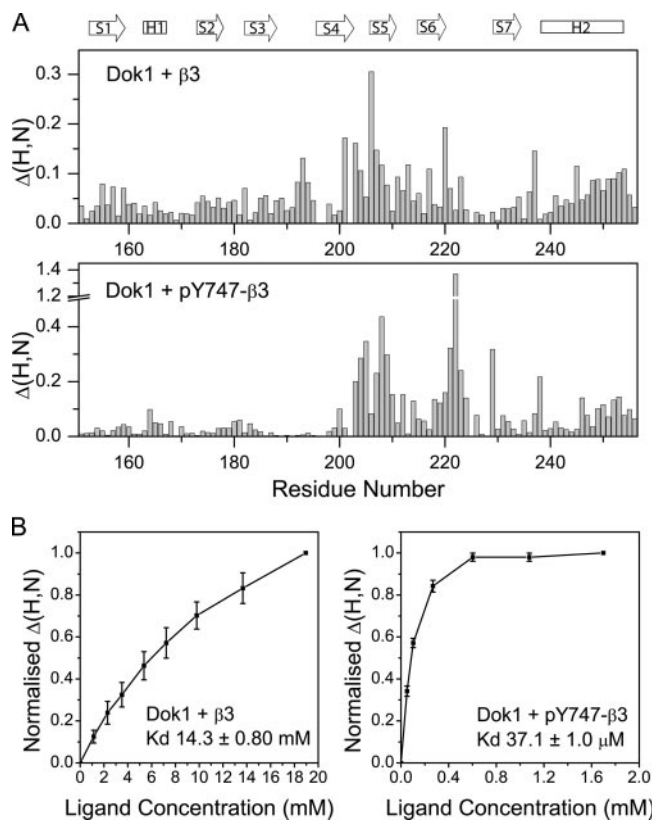

FIGURE 1. **NMR titration studies using the ^{15}N-labeled full-length β3 integrin tail.** *A*, a weighted shift map (see "Experimental Procedures") of induced chemical shift changes observed in ^{15}N-^{1}H HSQC spectra upon the addition of Dok1 PTB domain to the ^{15}N-labeled β3 integrin tail. *B*, averaged normalized weighted shifts, plotted against protein concentration, for full-length β3 integrin titrations with Dok1 and talin PTB domains. *Error bars* indicate the standard deviations for each titration point. Dissociation constants, K_d, calculated from the curves, are also shown.

sistent with Dok1 existing in a monomeric state. Two peptides were tested, each having the sequence [736]RAKWDTAN-NPLYKE[749], but with the second peptide phosphorylated at Tyr-747.

Titration with the unphosphorylated integrin peptide revealed chemical shift perturbations to residues from strand β5, the loop between strands β6 and β7 and along the C-terminal α-helix (Fig. 2A). The pattern of perturbations is similar to that found for the talin PTB domain binding to the same peptide (16), indicating a similar mode of interaction, with a dissociation constant of 14.3 ± 0.80 mM (Fig. 2B). In contrast, titration with the pTyr[747] phospho-peptide produced larger chemical shift changes (Fig. 2A), particularly in the region surrounding the canonical NP*XY* peptide binding pocket. Residue Arg[222], which contacts a sulfate ion in the crystal structure (*vide infra*), had the greatest perturbation. The dissociation constant for this interaction was calculated as 37 ± 1.0 μM, a 400-fold increase in affinity when compared with the unphosphorylated peptide (Fig. 2B).

Talin PTB Binding to β3 Integrin Tail and to Tyr(P)-747 β3 Integrin Tail—NMR was again used to study the effect of β-integrin Tyr[747] phosphorylation on binding to the talin PTB domain. The backbone resonances of the talin PTB domain have been assigned previously (16). Two ^{1}H-^{15}N HSQC titrations were performed using the same phosphorylated and unphosphorylated peptides as used in the Dok1 experiments.

The phosphorylated peptide perturbed similar residues to those affected by the unmodified peptide, with the strongest chemical shifts once again observed in strand β5, the loop between strands β6 and β7 and the C-terminal α-helix (Fig. 3A). The magnitudes of the chemical shift changes suggest that

FIGURE 2. **NMR titration studies of the β3 integrin or pTyr[747] β3 integrin peptide with the ^{15}N-labeled Dok1 PTB domain.** *A,* weighted shift maps (see "Experimental Procedures") of induced chemical shift changes observed in ^{15}N-^{1}H HSQC spectra upon the addition of peptide to the ^{15}N-labeled Dok1 PTB domain. *B,* averaged normalized weighted shifts, plotted against peptide concentration. *Error bars* indicate the standard deviations for each titration point. Dissociation constants, K_d, calculated from the curves, are also shown.
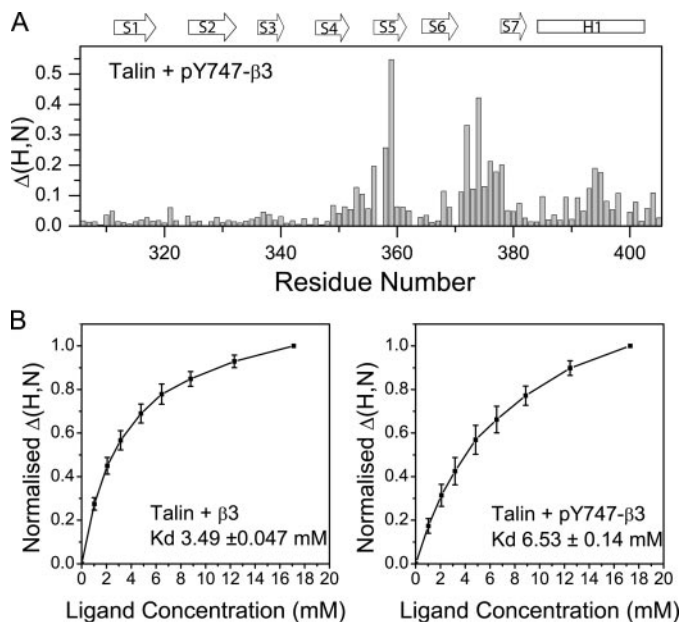
FIGURE 3. **NMR titration studies of the β3 integrin or pTyr[747] β3 integrin peptide with the ^{15}N-labeled talin PTB domain.** *A,* weighted shift maps (see "Experimental Procedures") of induced chemical shift changes observed in ^{15}N-^{1}H HSQC spectra upon the addition of pTyr[747] β3 integrin peptide to the ^{15}N-labeled talin PTB domain. *B,* averaged normalized weighted shifts for the titrations with the β3 and pTyr[747] β3 peptides, plotted against peptide concentration. *Error bars* indicate the standard deviations for each titration point. Dissociation constants, K_d, calculated from the curves, are also shown.

TABLE 1
Data collection and refinement statistics

Values in brackets represent last-resolution shell values. $R_{merge} = \sigma(I - \langle I \rangle)/\sigma I$; I and $\langle I \rangle$ are the intensity and the mean value of all the measurements of an individual reflection. *R*-factor $= \sum|F_o - F_c|/\sum|F_o|$; F_o and F_c are the observed and calculated structure factors. R_{free}; *R*-factor calculated for a randomly selected subset of reflections (5%) that were omitted during the refinement. r.m.s.d., root mean square deviation.

Data Collection	
Synchrotron source	ESRF ID14-EH2 s
Space Group	C2
Unit cell (Å, deg)	a = 76.88, b = 100.17, c = 67.10, β = 117.34
Resolution (Å)	25.98-1.6 (1.68-1.6)
No. of Reflections	447803
No. of unique reflections	59364
Completeness (%)	99.7 (98.3)
Multiplicity	7.5 (3.6)
Mean I/(I)	22.3 (2.5)
R_{merge} (%)	0.061 (0.383)
R_{pim} (within I+/I−)	0.02 (0.234)
Refinement statistics	
R-factor (%)	18.8
R_{free} (%)	22.4
r.m.s.d. from ideal geometry	
Bond lengths (Å)	0.017
Angles (deg)	1.557
Ramachandran plot	
Most favored region (%)	93
Additionally allowed (%)	7
Generously allowed (%)	0
Disallowed (%)	0

the pTyr[747] β3 integrin peptide binds more weakly to the talin PTB domain than to the unphosphorylated peptide. The dissociation constants were calculated to be 3.49 ± 0.047 mM for the unphosphorylated peptide and 6.53 ± 0.14 mM for the pTyr[747] phosphorylated integrin peptide (Fig. 3*B*). Thus, in contrast to the case for the Dok1 PTB domain, phosphorylation of the β3 integrin tail has a negative effect on affinity for the talin PTB domain.

Crystal Structure of the Human Dok1 PTB Domain—The crystal structure of the human Dok1 PTB domain was solved by molecular replacement at 1.6 Å. Data collection and refinement statistics are given in Table 1. The Dok1 PTB domain is comprised of seven β strands, a 3_{10} turn between β strands 4 and 5, and two α-helixes, of which the first α-helix is truncated. The seven β strands form a β sandwich comprised of two almost orthogonal antiparallel β sheets. The sandwich is capped by the C-terminal α-helix, whereas the second α-helix is inserted between strands 1 and 2. This is a typical fold for a PTB domain of the IRS group (29). The crystal asymmetric unit contains four copies of the Dok1 PTB domain, termed A, B, C, and D, superimposing with an root mean square deviation of 0.20 Å.

For chain A, electron density was observed for residues 2–104, but density was absent for residues 42–45, which are located in a loop between β-strands 3 and 4. For chain B and C, residues 5–106 were identified, and for chain D, electron density was observed for residues 5–103. Three of the four molecules (A, B, and D) associate with a sulfate ion accommodated in a positively charged pocket formed by Arg[222] and Arg[207] (Fig. 4*A*).

Structural Modeling of the pTyr[747] β3 Integrin Tail-Dok1 PTB Domain Interaction—Attempts to co-crystallize Dok1 PTB with the pTyr-747 β3 integrin tail produced crystals twinned to 43% and were thus not solved. To obtain a structural
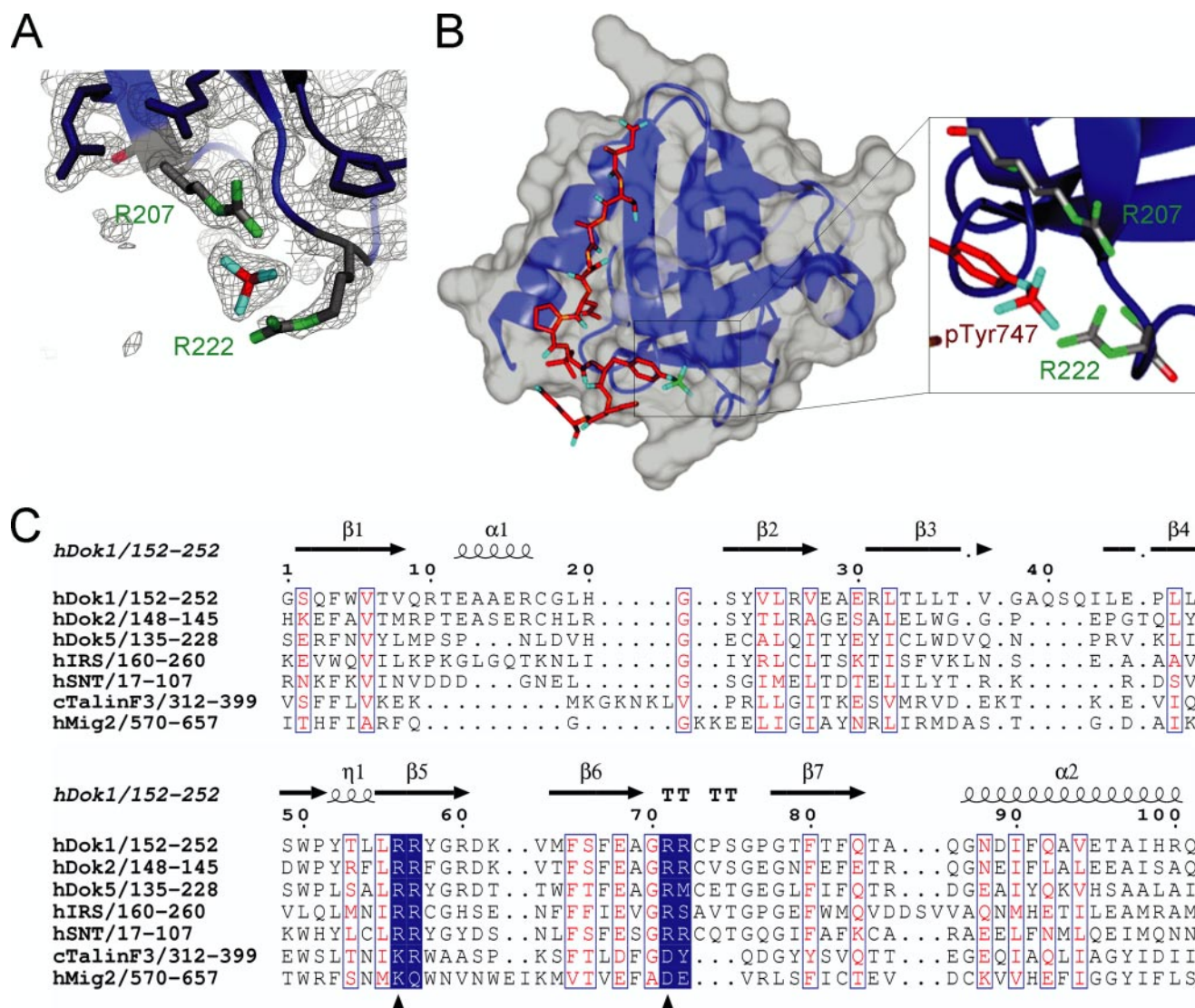
FIGURE 4. **Dok1 PTB binding to the phosphorylated β3 integrin tail is mainly mediated by two conserved arginines.** *A*, electron density map shown at 1.6 Å resolution covering Arg[222], Arg[207], and a sulfate molecule. The prefix *h* signifies human sequences, whereas *c* signifies chicken. *B*, model of the Dok1 PTB domain complexed with a peptide of the Tyr[747]-phosphorylated β3 integrin tail. *C*, sequence alignment of PTB domains belonging to the IRS-like group (29).

model of the pTyr-747 β3 integrin tail-Dok1 PTB domain interaction, we used the human Dok1 PTB domain crystal structure, as determined here, and the crystal structure of a complex between RET peptide and the mouse Dok1 PTB domain, as a template (1uef (21)). The RET peptide includes an NKLpY motif that binds the mouse Dok1 PTB domain in an analogous fashion to the canonical NP*XY*-PTB domain recognition mode (28). In our model, the phosphate group from integrin pTyr[747] is predicted to lie within hydrogen-bonding distance of the Arg[222] and Arg[207] of the side chains of Dok1 (Fig. 4*B*). These two residues, Arg[222] in particular, are strongly perturbed in the NMR spectra upon the addition of the pTyr-747 integrin peptide (Fig. 2*A*). In the crystal structure of the native Dok1 PTB domain, this position is occupied by a sulfate ion, suggesting that this region of Dok1 is a binding pocket for negatively charged groups.

The two key arginine residues that coordinate the phosphate moiety are conserved in PTB domains of the IRS-like group as classified by Uhlik *et al.* (29) (Fig. 4*C*). Exceptions to this are the talin and MIG-2 PTB domains, which have aspartic acid resi-

dues at the position corresponding to Arg[222] in Dok1. This observation is consistent with the affinity values in our NMR studies of the talin PTB-β3 integrin tail interaction.

DISCUSSION

Binding of β3 integrin tails to talin is the final step in integrin activation (15). The key molecular interaction required for activation is direct contact between the talin PTB domain and the membrane-proximal region of the β3 integrin tail (7). It has also been shown, using a cell-based functional assay, that Dok1 negatively regulates integrin activation. Here we show that the Dok1 PTB domain binds exclusively to the central NPLY motif of the wild-type full-length β3 integrin tail and does not make contact with the membrane-proximal residues. Thus, Dok1 is expected to compete with talin for the NPLY binding site but not to cause activation due to the lack of interaction with the membrane-proximal region.

We have also shown here that β3 integrin tail fragments containing the NPLY region have a 3-fold higher affinity for talin

than they do for Dok1. Utilizing the full integrin tail peptide increases the affinity for talin to 223 ± 5 μM due to additional interactions with membrane-proximal residues. However, tail interactions with Dok1 remain at a millimolar level.

How then can Dok1 negatively regulate integrin activation? One possibility is that the effects seen in the cell-based assays were introduced by the transfection system itself. Another explanation is the involvement of phosphorylation. There is evidence from previous studies that Dok1 ligand binding is phosphorylation-dependent; for example, the Dok1 PTB domain has been proposed as a phosphorylation-dependent negative regulator of T cell receptor signaling (30) Immunoprecipitation and immunoblotting experiments also point to a phosphorylation-dependent association of Dok1 with the β3 integrin tail (31).

Previous studies have hinted at the biological importance of β3 integrin tyrosine phosphorylation, particularly at Tyr^{747}. Mutation of Tyr^{747} to a non-phosphorylatable phenylalanine disrupted adhesion and clot retraction in hematopoietic cells, indicating that phosphorylation is important for normal integrin function in these cells (32). Although the Y783F/Y795F β1 tail mutations in the mouse have a mild phenotype (33), the corresponding Y747F/Y759F β3 integrin knock-in mouse has demonstrated disrupted platelet signaling manifested as a bleeding defect (34). It has previously been shown that tyrosine phosphorylation of the β3 integrin tail decreases the affinity of αVβ3 for its extracellular ligand fibronectin (35). Additional studies have indicated a role for β3 tyrosine phosphorylation in Rho family GTPase signaling pathways, which play a fundamental role in cytoskeletal organization (36, 37). Our data, taken together with these studies, not only highlight the role of integrin tyrosine phosphorylation in the cell but also indicate the targeted nature of this modification, manifested as a switch for integrin activation.

Our peptide titration studies with β3 integrin tail fragments, containing either the phosphorylated or the unphosphorylated NPLY recognition motif, clearly show that the unphosphorylated integrin tail has a 3-fold preference for the talin PTB domain, over that of Dok1. Phosphorylation of Tyr^{747}, however, enhances binding to Dok1 ~400-fold (from 14.3 mM to 37 μM), whereas the binding affinity to the talin PTB domain decreases by 2-fold (from 3.49 to 6.53 mM). Thus, phosphorylation of Tyr^{747} switches the binding preference of the integrin tail from talin to the Dok1 PTB domain. Tyrosine phosphorylation of the β-tail thus allows Dok1 to compete strongly with talin, and this would result in down-regulation of integrin activation. These results agree with previous studies that found a phosphorylation-dependent association of Dok1 with the β3 integrin tail (31) and suggestions that integrin β tail phosphorylation blocks talin binding (38).

PTB domains can be divided into three classes according to their structures and ligand binding preferences (29). Both the Dok1 and the talin PTB domains fit into the IRS-1-like group, which have a basic pleckstrin homology domain core structure, when compared with the Shc- and Dab-like PTB domains, which have additional α-helices, one at the N terminus and one inserted between β-strands 1 and 2. PTB domains in general show a preference for either phosphotyrosine or tyrosine in the

NP*XY* binding motif, and domains of the IRS-1-like group tend to prefer phosphorylated ligands.

Alignment of the PTB domains of various Dok homologues with other members of the IRS-1-like group (Fig. 4*C*) reveals several conserved arginine residues. The structural studies here suggest that Arg^{207} and Arg^{222} of that human Dok1 PTB (Fig. 4) form a pocket for negatively charged groups. Construction of a model of the interaction of phosphorylated integrin tail with Dok1 predicts that the pTyr^{747} phosphate group occupies this basic pocket and that the preference for phosphorylated ligands is due to these conserved arginine residues.

The talin PTB domain is also structurally categorized as IRS-1-like. However, unlike other IRS-1-like PTB domains, it shows a preference for unphosphorylated ligands. Competition assays using gel filtration (38) and glutathione *S*-transferase pull-downs (39) previously indicated a preference for unphosphorylated β1 integrins. Our quantitative results with β3 integrin confirm this preference. From the alignment in Fig. 4, this preference is likely to be due to the presence of an aspartic acid residue in the tyrosine binding pocket that would electrostatically disfavor phosphate binding. Evidence has recently emerged that the protein mitogen inducible gene-2 (MIG-2), also known as Kindlin-2, promotes integrin activation as well, although to a lesser degree than talin (40). Interestingly, MIG-2, like talin, has an aspartic acid residue in the tyrosine binding pocket (Fig. 4), suggesting that MIG-2 would also bind preferentially to unphosphorylated integrin tails. This prediction is consistent with the integrin tyrosine phosphorylation switch hypothesis presented here, indicating that tyrosine phosphorylation could be a common mechanism for regulating integrin activation states.

REFERENCES

1. Hynes, R. O. (2002) *Cell* **110,** 673–687
2. Hynes, R. O. (1987) *Cell* **48,** 549–554
3. Liu, S., Calderwood, D. A., and Ginsberg, M. H. (2000) *J. Cell Sci.* **113,** 3563–3571
4. Calderwood, D. A. (2004) *J. Cell Sci.* **117,** 657–666
5. Hutchinson, E. G., and Thornton, J. M. (1994) *Protein Sci.* **3,** 2207–2216
6. Eck, M. J., Dhe-Paganon, S., Trub, T., Nolte, R. T., and Shoelson, S. E. (1996) *Cell* **85,** 695–705
7. Wegener, K. L., Partridge, A. W., Han, J., Pickford, A. R., Liddington, R. C., Ginsberg, M. H., and Campbell, I. D. (2007) *Cell* **128,** 171–182
8. Yamanashi, Y., and Baltimore, D. (1997) *Cell* **88,** 205–211
9. Noguchi, T., Matozaki, T., Inagaki, K., Tsuda, M., Fukunaga, K., Kitamura, Y., Kitamura, T., Shii, K., Yamanashi, Y., and Kasuga, M. (1999) *EMBO J.* **18,** 1748–1760
10. Carpino, N., Wisniewski, D., Strife, A., Marshak, D., Kobayashi, R., Stillman, B., and Clarkson, B. (1997) *Cell* **88,** 197–204
11. Yasuda, T., Shirakata, M., Iwama, A., Ishii, A., Ebihara, Y., Osawa, M., Honda, K., Shinohara, H., Sudo, K., Tsuji, K., Nakauchi, H., Iwakura, Y., Hirai, H., Oda, H., Yamamoto, T., and Yamanashi, Y. (2004) *J. Exp. Med.* **200,** 1681–1687
12. Deleted in proof
13. Grimm, J., Sachs, M., Britsch, S., Di Cesare, S., Schwarz-Romond, T., Alitalo, K., and Birchmeier, W. (2001) *J. Cell Biol.* **154,** 345–354

14. Okada, K., Inoue, A., Okada, M., Murata, Y., Kakuta, S., Jigami, T., Kubo, S., Shiraishi, H., Eguchi, K., Motomura, M., Akiyama, T., Iwakura, Y., Higuchi, O., and Yamanashi, Y. (2006) *Science* **312,** 1802–1805

15. Tadokoro, S., Shattil, S. J., Eto, K., Tai, V., Liddington, R. C., de Pereda, J. M., Ginsberg, M. H., and Calderwood, D. A. (2003) *Science* **302,** 103–106

16. de Pereda, J. M., Wegener, K. L., Santelli, E., Bate, N., Ginsberg, M. H., Critchley, D. R., Campbell, I. D., and Liddington, R. C. (2005) *J. Biol. Chem.* **280,** 8381–8386

17. Wishart, D. S., Bigam, C. G., Yao, J., Abildgaard, F., Dyson, H. J., Oldfield, E., Markley, J. L., and Sykes, B. D. (1995) *J. Biomol. NMR* **6,** 135–140

18. Delaglio, F., Grzesiek, S., Vuister, G. W., Zhu, G., Pfeifer, J., and Bax, A. (1995) *J. Biomol. NMR* **6,** 277–293

19. Ayed, A., Mulder, F. A., Yi, G. S., Lu, Y., Kay, L. E., and Arrowsmith, C. H. (2001) *Nat. Struct. Biol.* **8,** 756–760

20. Collaborative Computational Project (1994) *Acta Crystallogr. Sect. D Biol. Crystallogr.* **50,** 760–763

21. Shi, N., Ye, S., Bartlam, M., Yang, M., Wu, J., Liu, Y., Sun, F., Han, X., Peng, X., Qiang, B., Yuan, J., and Rao, Z. (2004) *J. Biol. Chem.* **279,** 4962–4969

22. Read, R. J. (2001) *Acta Crystallogr. Sect. D Biol. Crystallogr.* **57,** 1373–1382

23. Emsley, P., and Cowtan, K. (2004) *Acta Crystallogr. Sect. D Biol. Crystallogr.* **60,** 2126–2132

24. Adams, P. D., Grosse-Kunstleve, R. W., Hung, L. W., Ioerger, T. R., Mc-Coy, A. J., Moriarty, N. W., Read, R. J., Sacchettini, J. C., Sauter, N. K., and Terwilliger, T. C. (2002) *Acta Crystallogr. Sect. D Biol. Crystallogr.* **58,** 1948–1954

25. Krissinel, E., and Henrick, K. (2004) *Acta Crystallogr. Sect. D Biol. Crystallogr.* **60,** 2256–2268

26. Schwede, T., Kopp, J., Guex, N., and Peitsch, M. C. (2003) *Nucleic Acids Res.* **31,** 3381–3385

27. Gouet, P., Courcelle, E., Stuart, D. I., and Metoz, F. (1999) *Bioinformatics (Oxf.)* **15,** 305–308

28. Forman-Kay, J. D., and Pawson, T. (1999) *Curr. Opin. Struct. Biol.* **9,** 690–695

29. Uhlik, M. T., Temple, B., Bencharit, S., Kimple, A. J., Siderovski, D. P., and Johnson, G. L. (2005) *J. Mol. Biol.* **345,** 1–20

30. Yasuda, T., Bundo, K., Hino, A., Honda, K., Inoue, A., Shirakata, M., Osawa, M., Tamura, T., Nariuchi, H., Oda, H., Yamamoto, T., and Yamanashi, Y. (2007) *Int. Immunol.* **19,** 487–495

31. Ling, Y., Maile, L. A., Badley-Clarke, J., and Clemmons, D. R. (2005) *J. Biol. Chem.* **280,** 3151–3158

32. Blystone, S. D., Williams, M. P., Slater, S. E., and Brown, E. J. (1997) *J. Biol. Chem.* **272,** 28757–28761

33. Czuchra, A., Meyer, H., Legate, K. R., Brakebusch, C., and Fassler, R. (2006) *J. Cell Biol.* **174,** 889–899

34. Law, D. A., DeGuzman, F. R., Heiser, P., Ministri-Madrid, K., Killeen, N., and Phillips, D. R. (1999) *Nature* **401,** 808–811

35. Datta, A., Huber, F., and Boettiger, D. (2002) *J. Biol. Chem.* **277,** 3943–3949

36. Gao, C., Schaefer, E., Lakkis, M., and Blystone, S. D. (2005) *J. Biol. Chem.* **280,** 15422–15429

37. Chandhoke, S. K., Williams, M., Schaefer, E., Zorn, L., and Blystone, S. D. (2004) *J. Cell Sci.* **117,** 1431–1441

38. Tapley, P., Horwitz, A., Buck, C., Duggan, K., and Rohrschneider, L. (1989) *Oncogene* **4,** 325–333

39. Ling, K., Doughman, R. L., Iyer, V. V., Firestone, A. J., Bairstow, S. F., Mosher, D. F., Schaller, M. D., and Anderson, R. A. (2003) *J. Cell Biol.* **163,** 1339–1349

40. Shi, X., Ma, Y. Q., Tu, Y., Chen, K., Wu, S., Fukuda, K., Qin, J., Plow, E. F., and Wu, C. (2007) *J. Biol. Chem.* **282,** 20455–20466